Nuclear Instruments and Methods in Physics Research A 694 (2012) 224–233

Contents lists available at SciVerse ScienceDirect

Nuclear Instruments and Methods in Physics Research A

journal homepage: www.elsevier.com/locate/nima

Focusing properties of a square electrostatic rainbow lens

I. Telečki [a], S. Petrović [a,*], P. Beličev [a], B. Rađenović [b], R. Balvanović [a], B. Bojović [a], N. Nešković [a]

[a] Vinča Institute of Nuclear Sciences, University of Belgrade, P.O. Box 522, 11001 Belgrade, Serbia
[b] Institute of Physics, University of Belgrade, Pregrevica 118, 11080 Belgrade, Serbia

ARTICLE INFO

Article history:
Received 3 April 2012
Received in revised form
1 August 2012
Accepted 19 August 2012
Available online 27 August 2012

Keywords:
Ion beam dynamics
Lenses
Rainbows

ABSTRACT

This paper is devoted to the focusing properties of a square electrostatic rainbow lens, which is a novel ion beam optical element. We consider the transmission of parallel and non-parallel proton beams of the initial kinetic energy of 10 keV through this lens. The potential of the electrodes of the lens is chosen to be 2 kV. The electrostatic potential and components of the electric field in the region of the lens are calculated using a three-dimensional finite element computer code. We investigate the spatial and angular distributions of protons propagating through the lens and in the drift space after it. It is confirmed that the evolutions of these distributions are determined by the evolutions of the corresponding rainbow lines, generated using the theory of crystal rainbows. The beam is separated into two components. One beam component, appearing as a beam core, is generated dominantly by the focused protons. Its boundary line in the transverse position plane can be very well approximated by a hypotrochoid. The other beam component is generated dominantly by the defocused protons. We present the focusing coefficient of the lens, the confining coefficients of the lens for the focused and defocused protons, the density of the beam core, the vertical or horizontal emittance of the beam core, and the brightness of the beam core.

1. Introduction

Four identical, parallel and positively charged cylindrical electrodes in vacuum whose axes pass through the apices of a square constitute a square electrostatic rainbow lens. Such an ion beam optical element was recently studied for the first time by Nešković et al. [1]. They analyzed the transmission of protons of the initial kinetic energy of 10 kV through the lens. The initial proton velocity vectors were parallel to the lens axis, i.e., the initial proton beam was parallel. The potential of the electrodes was chosen to be 10, 20, 50 and 100 kV. It was assumed that the electrostatic potential inside the lens could be approximated with the potential generated by the uniformly charged infinite straight wires lying along the electrode axes, and that the components of the electric field before and after the lens were equal to zero.

In our previous study [1], we explored the spatial distributions of transmitted protons inside the lens and in the drift space after it. It was demonstrated that the evolution of the spatial distribution was determined by the evolution of the corresponding rainbow pattern. The proton beam after the lens was clearly separated into the bright and dark components, corresponding to the bright and dark sides of the rainbow, respectively. All the focused protons were confined within the rainbow line. The effect was named the catastrophic ion beam focusing. We also explored the angular distributions of transmitted protons at the lens exit. The corresponding rainbow patterns appeared only when the potentials of the electrodes were 50 and 100 kV. In those cases, almost all the focused protons were confined within the rainbow line. Thus, the lens enabled one to create a proton beam core, which included the protons focused in both the transverse position plane and transmission angle plane.

This study is a continuation of our previous study [1]. The initial proton kinetic energy will also be $E_0=10$ kV. However, the initial proton beam will be parallel as well as non-parallel. The potential of the electrodes will be $\varphi_0=2$ kV. The electrostatic potential in the region of the lens will be calculated using a three-dimensional finite element computer code. We shall present the spatial and angular distributions of protons propagating through the lens and in the drift space after it, together with the corresponding rainbow lines, and describe in detail the transmitted non-parallel beam.

2. Square electrostatic rainbow lens

Fig. 1 gives a three-dimensional view of the square electrostatic rainbow lens under consideration together with its transverse and longitudinal sections. These drawings belong to the conceptual design documentation of the lens, which was prepared within this study. The outer diameter of each electrode of the lens is $2a_e=80$ mm and its length is $L_e=400$ mm. The distance

* Corresponding author. Tel.: +381 11 2454 965; fax: +381 11 2447 963.
E-mail address: petrovs@vinca.rs (S. Petrović).

0168-9002/$ - see front matter © 2012 Elsevier B.V. All rights reserved.
http://dx.doi.org/10.1016/j.nima.2012.08.051

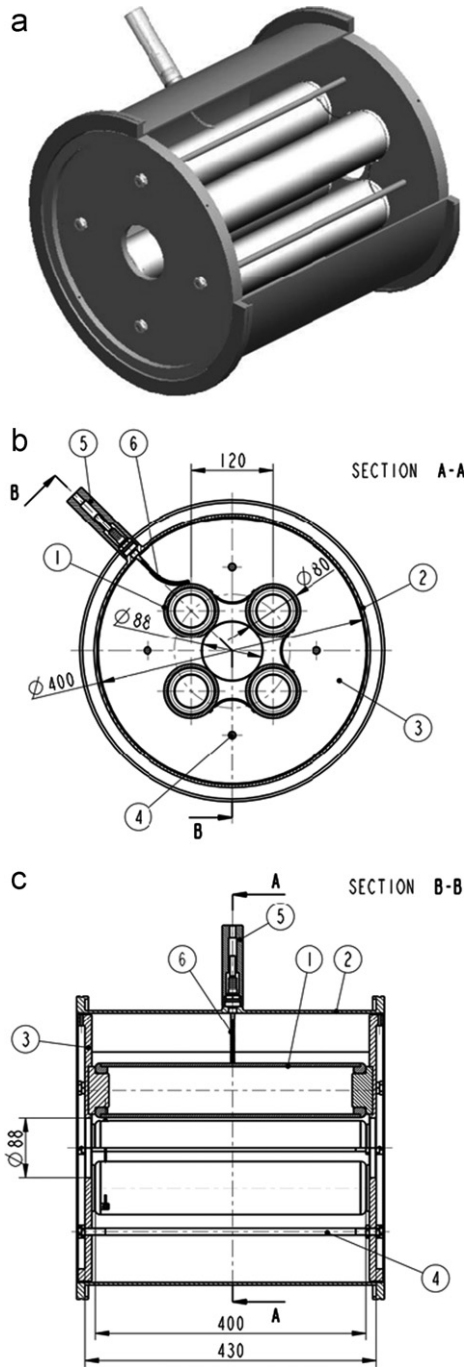

Fig. 1. (a) A three-dimensional view of the square electrostatic rainbow lens, (b) its transverse section—A-A, and (c) its longitudinal section—B-B: 1—the electrode with the insulating buttons, 2—the boundary cylinder, 3—the boundary plate with the aperture, 4—the connecting rod, 5—the electrical feedthrough, and 6—the electrical connector.

between the axes of the neighboring electrodes is $b_e=120$ mm. The inner diameter of the boundary cylinder of the lens, which is grounded, is $2a_c=400$ mm. The entrance and exit boundary plates have the circular shapes. The distance between the entrance plane of the entrance plate and the exit plane of the exit plate, being the entrance and exit planes of the lens, is $L_p=430$ mm. The diameters of the apertures within the entrance and exit plates, being the entrance and exit apertures of the lens, are $2a_p=88$ mm. The electrodes are connected to the entrance and exit plates via the insulating buttons, while the plates are connected to each other with the connecting rods. The electrodes, boundary cylinder, entrance and exit plates, and connecting rods are made of stainless steel. The electrodes are connected to a high voltage power supply via an electrical feedthrough and four electrical connectors. The producer of the power supply is FuG, its type is HCP 140-20000, and its maximal output voltage is 20 kV. The producer of the electrical feedthrough is MDC and its type is SHV-20. The electrical circuit of the lens also includes 13 serial resistors in series with three parallel resistors placed in parallel with the power supply. The producer of the resistors is Multicomp and their type is 2 W 5% 1M5.

3. Theory

In this study the z axis of the reference frame is taken to coincide with the lens axis with the origin lying in the median plane of the lens. The x and y axes of the reference frame are the vertical and horizontal axes, respectively.

3.1. Electrostatic potential

The electrostatic potential and components of the electric field in the region of the lens are calculated using the GetDP computer code [2], being a general finite element solver. It is based on a thorough implementation of the discrete differential forms calculus, and employs the mixed finite elements to discretize the de Rham type complexes in one, two and three dimensions. The meshing of the computational domain is carried out by the TetGen tetrahedral mesh generator [3]. It generates the boundary constrained high quality Delaunay meshes, suitable for numerical simulation using the finite element and finite volume methods.

The Laplace equation corresponding to the electrostatic problem in question is solved using the second order hierarchic nodal basis functions and h-adaptive procedure. The original computational domain is a parallelepiped of the transverse dimensions of $A_d=B_d=400$ mm and the longitudinal dimension of $C_d=510$ mm. However, taking into account the symmetry properties of the lens, the computation is performed in the reduced computational domain in which x and y vary between 0 and 200 mm and z between 0 and 255 mm, whose volume is eight times smaller than the volume of the original computational domain. An *a posteriori* energy-norm estimator is used to find the regions where the computation is performed with large errors, and to refine it in the next iteration. The target energy-norm error was set to 0.07%, and the resulting total number of tetrahedra in the reduced computational domain in the last iteration was 1,951,249.

3.2. Rainbow lines

As in our previous study [1], we are going to apply to the problem in question the theory of crystal rainbows [4–8]. It is assumed that the proton propagation angle inside the lens and in the drift space after it remains small. In order to obtain the components of the proton position and velocity vectors at the chosen point inside the lens or in the drift space after it, one must solve the proton equations of motion. We neglect the space charge effect, i.e., the obtained results are valid for small values of the initial proton beam current. The transverse components of the initial proton position vector are equal to the components of its impact parameter vector, designated as x_0 and y_0. The transverse components of the initial proton velocity vector are designated as v_{x0} and v_{y0}. The obtained transverse components of the proton position vector for the chosen value of z are $x(\vec{\rho}_0, \vec{v}_{\rho 0}, z)$ and $y(\vec{\rho}_0, \vec{v}_{\rho 0}, z)$, and the corresponding transverse and longitudinal components of the proton velocity vector are $v_x(\vec{\rho}_0, \vec{v}_{\rho 0}, z)$, $v_y(\vec{\rho}_0, \vec{v}_{\rho 0}, z)$ and $v_z(\vec{\rho}_0, \vec{v}_{\rho 0}, z)$, respectively, with $\vec{\rho}_0=(x_0, y_0)$ and $\vec{v}_{\rho 0}=(v_{x0}, v_{y0})$,

where z varies from the initial transverse position plane, being at $z=-C_d/2=-25.5$ cm, to the beginning of the drift space after the lens, being at $z=C_d/2=25.5$ cm, and further. The corresponding components of the proton transmission angle are $\theta_x(\vec{\rho}_0,\vec{v}_{\rho 0},z)=v_x/v$ and $\theta_y(\vec{\rho}_0,\vec{v}_{\rho 0},z)=v_y/v$, where $v(\vec{\rho}_0,\vec{v}_{\rho 0},z)=(v_x^2+v_y^2+v_z^2)^{1/2}$ is the corresponding magnitude of the proton velocity vector. The spatial distribution of transmitted protons for the chosen value of z, i.e., their distribution in the chosen transverse position plane, and the corresponding angular distribution, i.e., the corresponding distribution in the transmission angle plane, are generated by the Monte Carlo computer simulation method.

We have investigated the cases of parallel and non-parallel initial proton beams. In the case of parallel initial beam, the values of x_0 and y_0 are chosen randomly within the uniform distribution over the circle of diameter of 80 mm, being 8 mm smaller than the radius of the entrance lens aperture, and the values of $\theta_{x0}=v_{x0}/v_0$ and $\theta_{y0}=v_{y0}/v_0$, where v_0 is the magnitude of the initial proton velocity vector, are taken to be zero.

In the case of non-parallel initial proton beam, we assume that it initially has a double waist. In the transverse position plane, the initial beam is described by a two-dimensional Gaussian distribution centered at the origin and having the vertical and horizontal standard deviations equal to $x_{0m}/2$ and $y_{0m}/2$, with $x_{0m}=y_{0m}=40$ mm being its adopted vertical and horizontal spatial half-widths, respectively. Similarly, in the propagation angle plane, the initial beam is described by a two-dimensional Gaussian distribution centered at the origin and having the vertical and horizontal standard deviations equal to $\theta_{x0m}/2$ and $\theta_{y0m}/2$, with $\theta_{x0m}=\theta_{y0m}=5$ mrad being its adopted vertical and horizontal angular half-widths, respectively. The values of x_0, y_0, θ_{x0} and θ_{y0} are chosen using Eq. (71) in Ref. [9]. In accordance with the above adopted values of x_{0m}, y_{0m}, θ_{x0m} and θ_{y0m}, the vertical and horizontal emittances of the initial beam are equal to $\varepsilon_{0x}=\varepsilon_{0y}=\varepsilon_0=200$ mm mrad. The initial number of protons is 400,000. If during its propagation through the lens, the proton hits the entrance plate, one of the electrodes, the boundary cylinder or the exit plate, it is excluded from the calculation.

The mapping of the impact parameter plane to the transverse position plane is described by the Jacobian of the transverse components of the proton position vector, which reads

$$J_\rho(\vec{\rho}_0,\vec{v}_{\rho 0},z)=\partial_{x_0}x\partial_{y_0}y-\partial_{y_0}x\partial_{x_0}y \quad (1)$$

Equation $J_\rho(\vec{\rho}_0,\vec{v}_{\rho 0},z)=0$ should give the spatial rainbow lines in the impact parameter plane, along which this mapping is singular. If these lines exist, their images determined by functions $x(\vec{\rho}_0,\vec{v}_{\rho 0},z)$ and $y(\vec{\rho}_0,\vec{v}_{\rho 0},z)$ are the rainbow lines in the transverse position plane. On the other hand, the mapping of the impact parameter plane to the transmission angle plane is described by the Jacobian of the components of the proton transmission angle, which reads

$$J_\theta(\vec{\rho}_0,\vec{v}_{\rho 0},z)=\partial_{x_0}\theta_x\partial_{y_0}\theta_y-\partial_{y_0}\theta_x\partial_{x_0}\theta_y \quad (2)$$

Equation $J_\theta(\vec{\rho}_0,\vec{v}_{\rho 0},z)=0$ should give the angular rainbow lines in the impact parameter plane, along which this mapping is singular. If these lines exist, their images determined by functions $\theta_x(\vec{\rho}_0,\vec{v}_{\rho 0},z)$ and $\theta_y(\vec{\rho}_0,\vec{v}_{\rho 0},z)$ are the rainbow lines in the transmission angle plane. If they appear, the rainbow lines in the transverse position plane and transmission angle plane separate the bright and dark regions in these planes.

4. Results and discussion

As we have said above, in our previous study [1], we approximated the electrodes of the lens with the uniformly charged infinite wires and assumed that the components of the electric field before and after the lens were equal to zero. Inside the lens, the transverse components of the electric field depended only on x and y and its longitudinal component was equal to zero. Thus, a proton propagating through the lens did not experience any longitudinal component of the force, and the longitudinal component of its velocity did not change. However, if one takes the realistic electrostatic potential in the whole region of the lens, as we do in this study, the proton experiences all three components of the electric field, which vary transversally as well as longitudinally. As a result, in the region before the median plane of the lens the longitudinal proton kinetic energy is decreased, and in the region after this plane it is increased, but only if it is not stopped and turned back before it reaches this plane. If the proton is transmitted through the lens, its final kinetic energy, in the drift space after the lens, is the same as its initial kinetic energy, in the drift space before the lens. The possibility that the proton is transmitted through the lens depends on its initial kinetic energy, the transverse components of its initial position and velocity vectors, and the potential of the electrodes.

Fig. 2a and b show the electrostatic potentials in the three-dimensional representation inside the lens in its median plane, for $z=0$, and for $z=15$ cm, respectively, with $\varphi_0=2$ kV. It demonstrates how the depth of the potential well in which the protons move changes along the lens.

4.1. Parallel beam

Let us first take that the initial proton beam is parallel. Fig. 3 gives the transmission coefficient of the lens, k_t, as a function of z for φ_0 varying between 2 and 10 kV with the step of 2 kV. This parameter of the lens is defined as the ratio of the number of transmitted protons in the beginning of the drift space after the lens and the initial number of protons, i.e., for $z=25.5$ and -25.5 cm, respectively. One should note that for each value of φ_0, k_t has a sudden decrease for z between -21.5 and 20 cm, i.e., between the entrance plane of the lens and the entrance ends of the electrodes. For $\varphi_0=2$, 4, 6 and 8 kV, k_t has an additional sudden decrease for z between 20 and 21.5 cm, i.e., between the exit ends of the electrodes and the exit plane of the lens. The former effect occurs in the region of the entrance stray electric field of the lens and the latter effect in the region of its exit stray field. For $\varphi_0=2$ kV, k_t falls to 0.820 and for $\varphi_0=10$ kV, to a value very close to zero in the beginning of the drift space after the electrodes. In order to study in detail the parameters of the transmitted beam, we have chosen the value of φ_0 to be 2 kV, resulting in a high final value of k_t.

We have analyzed the spatial distributions of transmitted protons inside the lens, for $z=-10$, 0 and 10 cm, and at its exit, for $z=21.5$ cm. Each of these distributions has two parts, the former part generated dominantly by the focused protons and the latter part by the defocused protons [1]. The focused protons are those whose distances from the lens axis do not increase. They satisfy condition $xv_x+yv_y\le 0$. The distances from the lens axis of the defocused protons increase. They satisfy condition $xv_x+yv_y>0$. These conditions are more general than the corresponding ones given in Ref. [1]. As one can expect, the focused protons are distributed around the lines connecting the opposite electrodes, and the defocused protons around the lines between the neighboring electrodes. For $z=-10$ cm there is no rainbow line in the transverse position plane. This is because in this case, the spatial rainbow line in the impact parameter plane lies outside the entrance lens aperture [1]. For $z=0$ four parts of a rainbow line appear, which correspond to the four parts of a spatial rainbow line in the impact parameter plane that have entered the entrance lens aperture [1]. For $z=10$ and 21.5 cm the

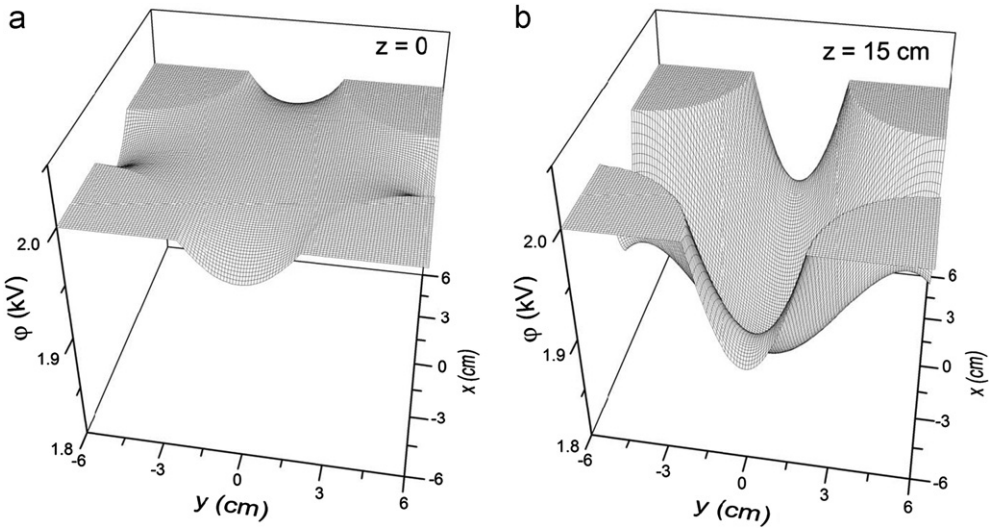

Fig. 2. Electrostatic potentials, $\varphi(x,y)$, in the three-dimensional representation inside the lens (a) in its median plane, for $z=0$, and (b) for $z=15$ cm with $\varphi_0=2$ kV.

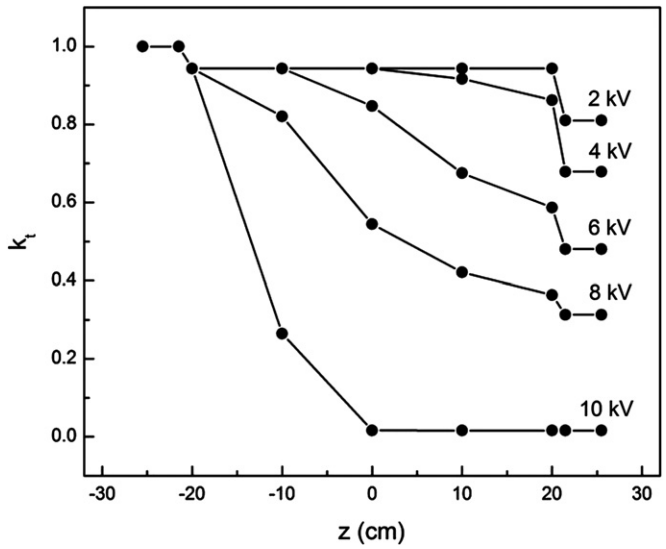

Fig. 3. Dependences of the transmission coefficient of the lens, k_t, on z for φ_0 varying between 2 and 10 kV with the step of 2 kV when the initial proton beam is parallel.

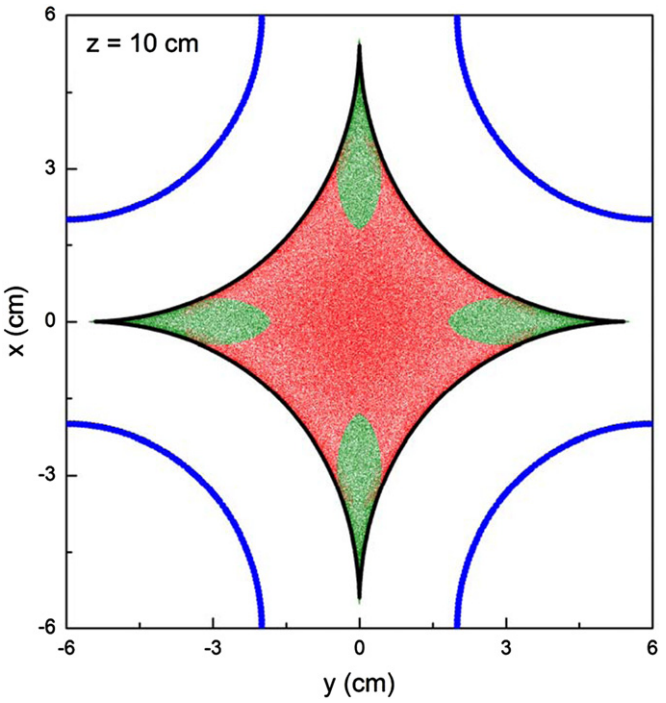

Fig. 4. Spatial distribution of transmitted protons in the two-dimensional representation inside the lens for $z=10$ cm with $\varphi_0=2$ kV when the initial proton beam is parallel. The red and green points designate the focused and defocused protons, respectively. The full black line is the rainbow line in the transverse position plane. The blue quarter-circles represent the surfaces of the electrodes. (For interpretation of references to color in this figure, the reader is referred to the web version of this article.)

rainbow lines are the cusped squares with the cusps directed between the electrodes [1].

The spatial distribution of transmitted protons in the two-dimensional representation for $z=10$ cm is given in Fig. 4. It is clear that the shape of the rainbow line fully determines the shape of this distribution. The analysis has shown that for $z=10$ cm the rainbow line bounds 99.8% of the focused protons and 97.2% of the defocused protons, while for $z=21.5$ cm these percentages are 99.5 and 62.9%, respectively. As one can expect, as z increases, the percentages of focused and defocused protons lying within the rainbow line decrease. However, the decrease of the percentage of defocused protons is much more pronounced.

Fig. 5 shows the angular distribution of transmitted protons in the two-dimensional representation in the beginning of the drift space after the lens, for $z=25.5$ cm. The focused and defocused protons are distributed in the whole vertical and horizontal angular regions between about -45 and 45 mrad (which is not seen in the figure). However, the focused protons are concentrated within the rainbow line, which is a cusped square with the cusps directed toward rather than between the electrodes [1]. One can say that the shape of the rainbow line determines the shape of this distribution. The analysis has shown that the rainbow line bounds 41.0% of the focused protons and 8.2% of the defocused protons.

4.2. Spatial and angular distributions

Let us now take that the initial proton beam is non-parallel. As in the case of parallel initial beam, the potential of the electrodes has been chosen to be $\varphi_0=2$ kV. The initial distribution of protons in the $x\theta_x$ plane, for $z=-25.5$ cm, is given in Fig. 6. In analyzing the distributions of focused and defocused protons in this figure,

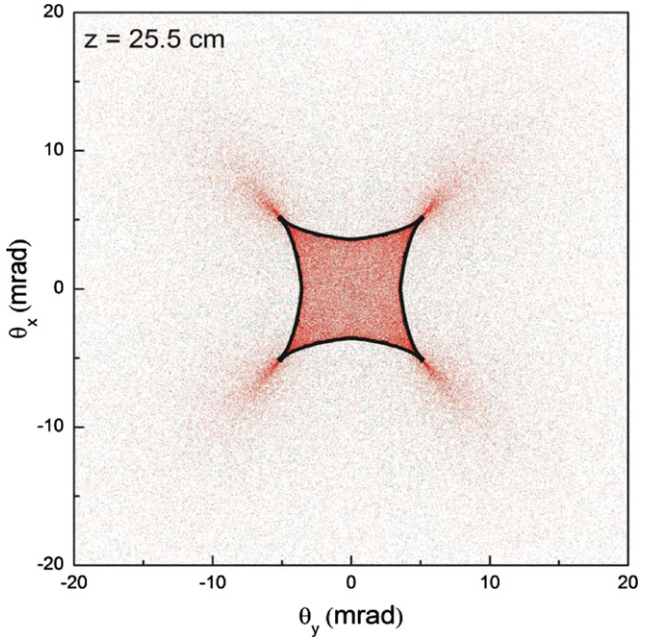

Fig. 5. Angular distribution of transmitted protons in the two-dimensional representation in the beginning of the drift space after the lens, for $z=25.5$ cm, with $\varphi_0=2$ kV when the initial proton beam is parallel. The red and green points designate the focused and defocused protons, respectively. The full black line is the rainbow line in the transmission angle plane. (For interpretation of references to color in this figure, the reader is referred to the web version of this article.)

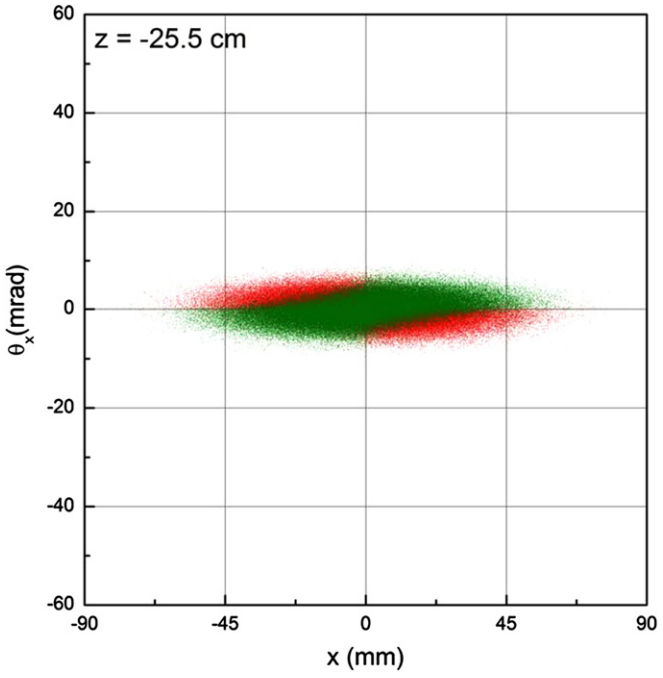

Fig. 6. Initial distribution of protons in the $x\theta_x$ plane, for $z=-25.5$ cm, with $\varphi_0=2$ kV when the initial proton beam is non-parallel. The red and green points designate the focused and defocused protons, respectively. (For interpretation of references to color in this figure, the reader is referred to the web version of this article.)

being designated by red and green points, respectively, one must not forget that the above mentioned conditions satisfied by the focused and defocused protons include both transverse components of the proton position vector, x and y, and both transverse components of the proton velocity vector, v_x and v_y.

As it has been stated above, in the case under consideration, the proton experiences all three components of the electric field during its propagation through the lens. These components vary transversally as well as longitudinally. This is especially pronounced in the entrance and exit regions of the lens, where the stray electric fields exist. The corresponding variation of the longitudinal proton kinetic energy is different for different sets of transverse components of the initial proton position and velocity vectors. Consequently, one can talk about the longitudinal kinetic energy distribution of protons propagating through the lens rather than about a single value of the longitudinal proton kinetic energy. Fig. 7 shows the longitudinal kinetic energy distributions of transmitted protons at the lens entrance, for

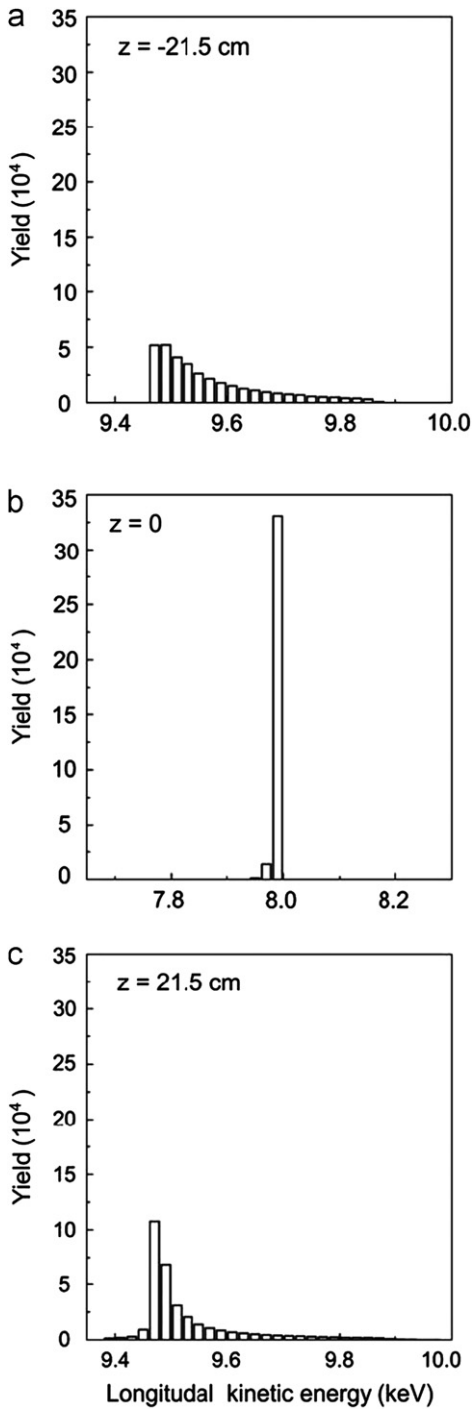

Fig. 7. Longitudinal kinetic energy distributions of transmitted protons (a) at the lens entrance, for $z=-21.5$ cm, (b) in its median plane, for $z=0$, and (c) at its exit, for $z=21.5$ cm, with $\varphi_0=2$ kV when the initial proton beam is non-parallel.

$z=-21.5$ cm, in its median plane, for $z=0$, and at its exit, for $z=21.5$ cm. For $z=-21.5$ cm, the span of the distribution is from 9.46 to 9.88 keV and its maximum at 9.49 keV, for $z=0$, the span is from 7.94 to 8.00 keV and the maximum at 7.99 keV, and for $z=21.5$ cm, the span is from 9.38 to 9.98 keV and the maximum at 9.47 keV.

The spatial distributions of transmitted protons inside the lens, for $z=-10$, 0 and 10 cm, and at its exit, for $z=21.5$ cm, are similar to the corresponding distributions when the initial proton beam is parallel. The chosen non-parallelism of the initial beam induces a moderate smearing of the distributions. This is demonstrated in Fig. 8. The rainbow lines shown in this figure are those calculated for the parallel initial beam. As it has been said above, the rainbow lines appear for $z=0$, 10 and 21.5 cm. The analysis has shown that for $z=10$ cm the rainbow line bounds 96.0% of the focused protons and 87.8% of the defocused protons, and that for $z=21.5$ cm these percentages are 92.0 and 45.7%, respectively. It is evident from the figure that as z increases, the focused and defocused protons move from the bright side of the rainbow to its dark side between its cusps and through them, respectively [1]. However, the moving of the defocused protons is much more pronounced.

Fig. 9 gives the spatial distributions of transmitted protons in the two-dimensional representation in the drift space after the lens for $z=31.5$, 41.5, 71.5 and 121.5 cm. Again, the rainbow lines are those calculated for the parallel initial proton beam. The analysis has shown that in this region the decreasing of the percentages of focused and defocused protons lying within the rainbow lines as z increases is faster than inside the lens. For $z=121.5$ cm these percentages are only 12.0 and 2.8%, respectively. It is evident that the beam is separated into two components. One beam component, appearing as a beam core, is generated dominantly by the focused protons and has the form determined by the form of the rainbow line. Its boundary line can be very well approximated by a hypotrochoid, which is given by

$$x = a[3\cos\varphi + \lambda\cos(3\varphi)] \tag{3}$$

and

$$y = a[3\sin\varphi - \lambda\sin(3\varphi)] \tag{4}$$

with $0<\varphi\le 2\pi$, where $a=(1/6)(\alpha+\sqrt{2}\beta)$ and $\lambda=3(\alpha-\sqrt{2}\beta)/(\alpha+\sqrt{2}\beta)$; the values of α and β are equal to the values of x for $\varphi=0$ and $\pi/4$, respectively, for which the yields of focused transmitted protons fall to 10% of the maximal yield, being at the origin. It should be noted that for $\lambda=1$ this line is a cusped square, also called astroid, and that for $\lambda=0$ it is a circle. This figure also gives the hypotrochoids bounding the beam cores for the four values of z. As z increases, the dimensions of the hypotrochoid decrease. However, one cannot see the tendency of reduction of this beam component to a point. This is attributed to the anharmonic character of the electrostatic potential [1]. The other beam component is generated dominantly by the defocused protons and has the form of a cross with the arms directed between the electrodes.

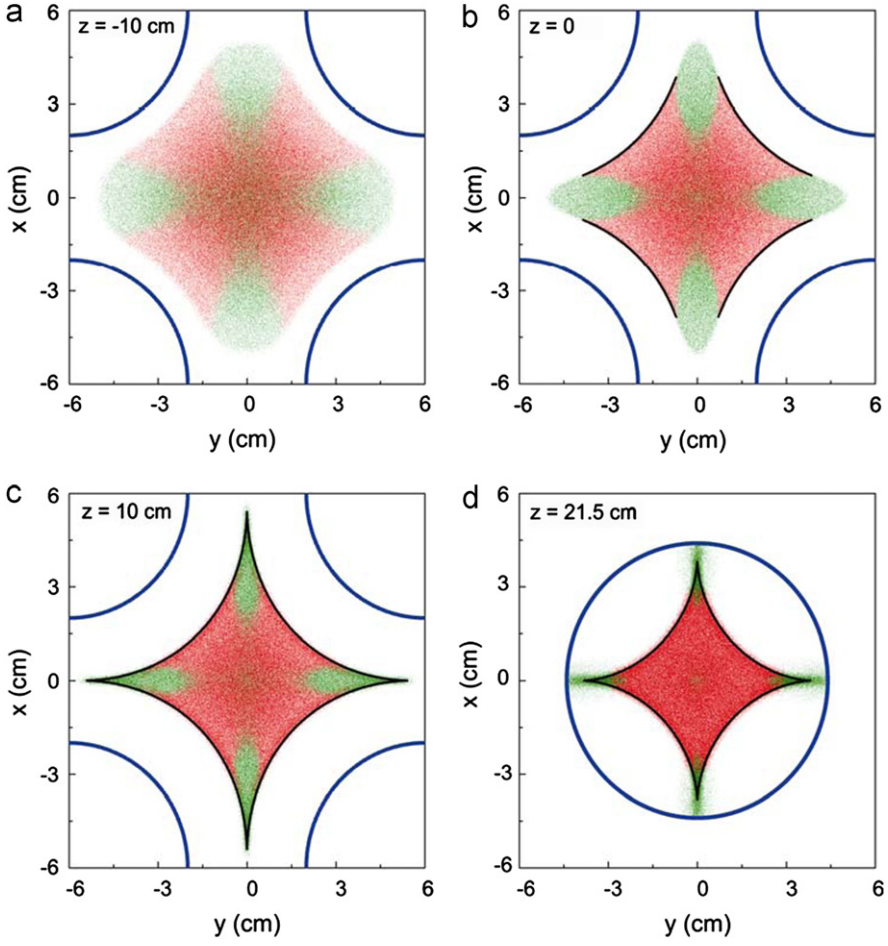

Fig. 8. Spatial distributions of transmitted protons in the two-dimensional representation inside the lens for (a) $z=-10$ cm, (b) $z=0$, and (c) $z=10$ cm, and (d) at its exit, for $z=21.5$ cm, with $\varphi_0=2$ kV when the initial proton beam is non-parallel. The red and green points designate the focused and defocused protons, respectively. The full black lines are the rainbow lines in the transverse position plane. The blue quarter-circles, appearing in (a), (b), and (c), represent the surfaces of the electrodes, while the blue circle, appearing in (d), represent the exit lens aperture. (For interpretation of references to color in this figure, the reader is referred to the web version of this article.)

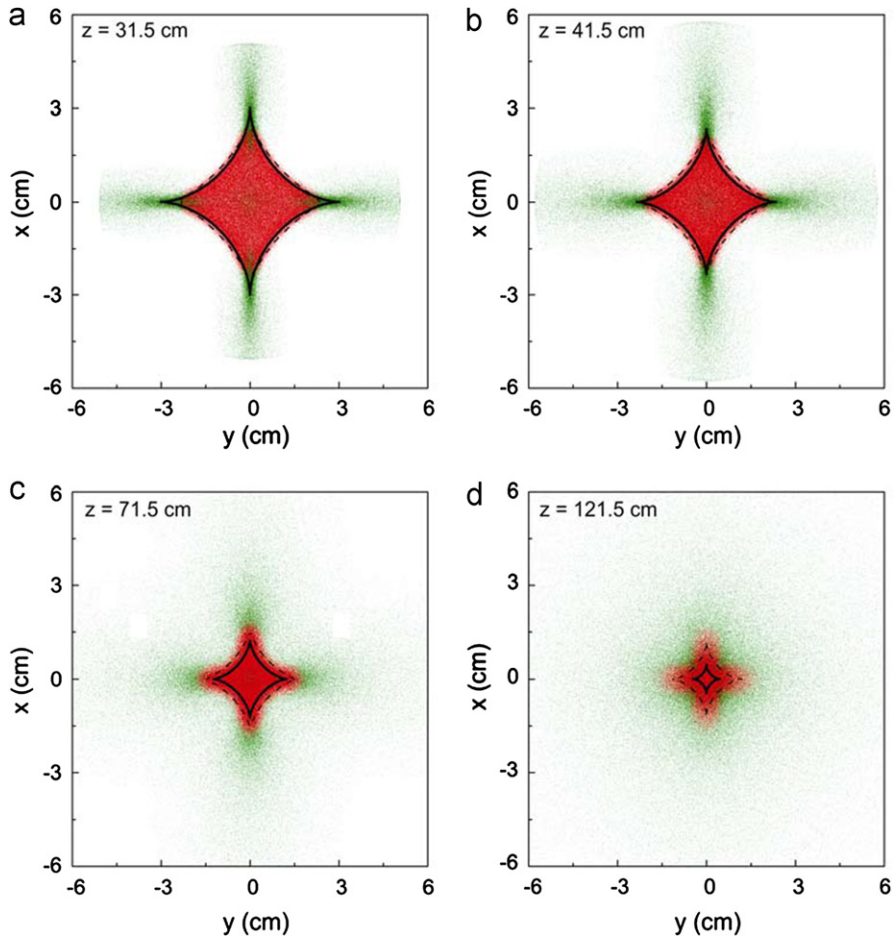

Fig. 9. Spatial distributions of transmitted protons in the two-dimensional representation in the drift space after the lens for (a) $z=31.5$ cm, (b) $z=41.5$ cm, (c) $z=71.5$ cm, and (d) $z=121.5$ cm with $\varphi_0=2$ kV when the initial proton beam is non-parallel. The red and green points designate the focused and defocused protons, respectively. The full black lines are the rainbow lines in the transverse position plane and the dashed black lines are the hypotrochoids defining the proton beam cores. (For interpretation of references to color in this figure, the reader is referred to the web version of this article.)

Fig. 10 shows the angular distribution of transmitted protons in the two-dimensional representation in the beginning of the drift space after the lens, for $z=25.5$ cm. Again, the rainbow line is the one calculated for the parallel initial proton beam. As in the case of parallel initial beam, the focused and defocused protons are distributed in the whole horizontal and vertical angular regions between about -45 and 45 mrad (which is not seen in the figure). In this distribution, there is no clear separation between the focused and defocused protons. However, one can say that the shape of the rainbow line determines the shape of the distribution. The analysis has shown that 26.2% of the focused protons and 11.9% of the defocused protons lie within the rainbow line.

The distribution of transmitted protons in the $x\theta_x$ plane in the beginning of the drift space after the lens, for $z=25.5$ cm, is given in Fig. 11. This distribution, when compared with the one given in Fig. 6, demonstrates clearly that the action of the lens is highly non-linear [10]. It should be noted that, because of the symmetry properties of the lens, this distribution coincides with the corresponding distribution of transmitted protons in the $y\theta_y$ plane.

Figs. 12 and 13 give the contour plots of the spatial and angular distributions of transmitted protons in the beginning of the drift space after the lens, for $z=25.5$ cm, respectively. The four maxima of the former distribution correspond to the apices of the cusps of the rainbow line in the transverse position plane. The distribution clearly demonstrates the catastrophic character of the proton beam dynamics in the lens [1]. The latter distribution has been already shown in Fig. 10. One can see clearly that both distributions have the hypotrochoidal forms with the former one being close to an astroid and the latter one changing toward a circle.

4.3. Beam parameters

We are now going to describe quantitatively the evolution of the initially non-parallel proton beam through the lens and in the drift space after it. Fig. 14 gives the focusing coefficient of the lens, k_f, as a function of z between -25.5 and 121.5 cm. This parameter of the lens is defined as the ratio of the number of focused protons in a transverse position plane and the initial number of protons [1]. As one can see, k_f decreases sharply in the region of the entrance stray electric field, increases sharply above its initial value, k_{f0}, decreases slightly and again increases sharply in the region of the electrodes, begins to decrease in the region of the exit stray field, and continues to decrease in the drift space after the lens, finally falling below k_{f0}. The behavior of k_f in the regions before and after the median plane of the lens can be attributed to the facts that in the former region the protons are decelerated and that in the latter region they are accelerated. This figure also shows the confining coefficients of the lens for the focused and defocused protons, k_{cf} and k_{cd}, respectively, on z between 10 cm, when the whole spatial rainbow line in the impact parameter plane lies inside the entrance lens aperture, and 121.5 cm. In analogy with the similar definitions given in Ref. [1], we define these parameters of the lens as the ratio of the number of focused

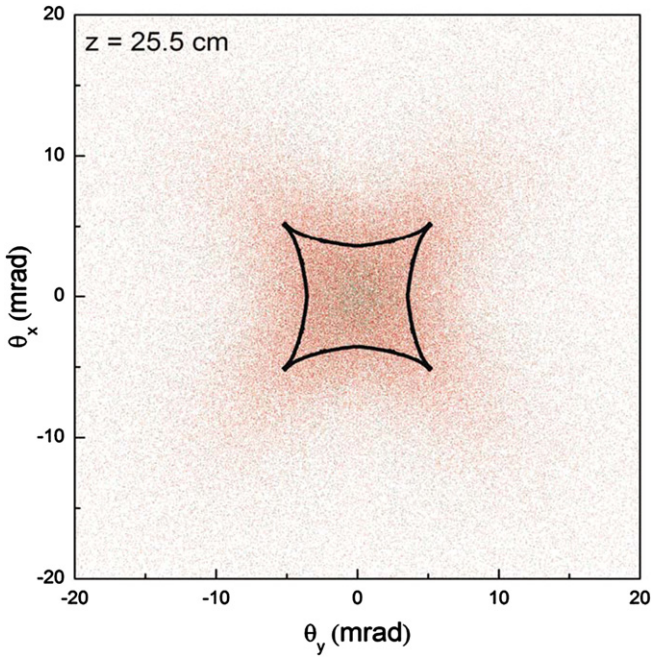

Fig. 10. Angular distribution of transmitted protons in the two-dimensional representation in the beginning of the drift space after the lens, for $z=25.5$ cm, with $\varphi_0=2$ kV when the initial proton beam is non-parallel. The red and green points designate the focused and defocused protons, respectively. The full black line is the rainbow line in the transmission angle plane. (For interpretation of references to color in this figure, the reader is referred to the web version of this article.)

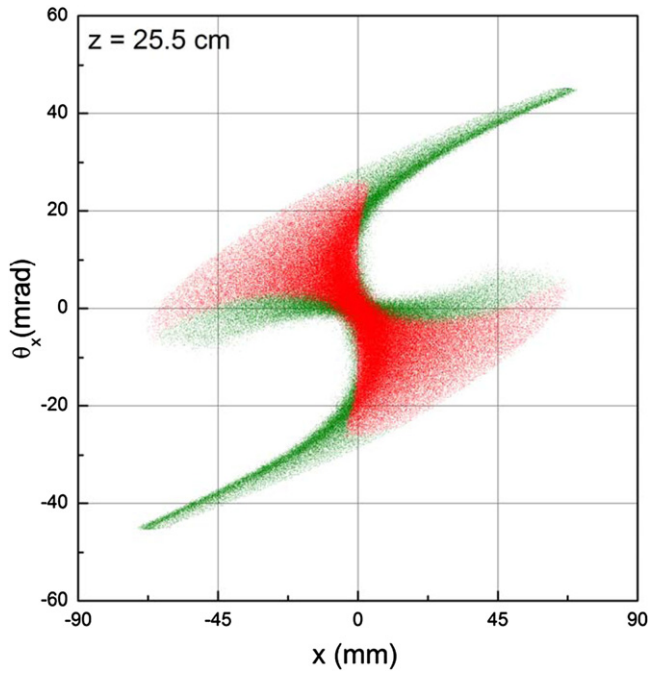

Fig. 11. Distribution of transmitted protons in the $x\theta_x$ plane in the beginning of the drift space after the lens, for $z=25.5$ cm, with $\varphi_0=2$ kV when the initial proton beam is non-parallel. The red and green points designate the focused and defocused protons, respectively. (For interpretation of references to color in this figure, the reader is referred to the web version of this article.)

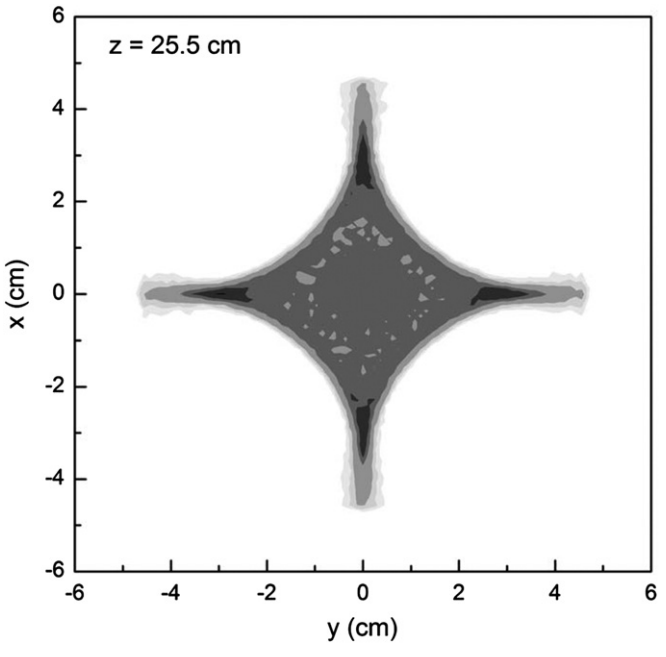

Fig. 12. Spatial distribution of transmitted protons in the two-dimensional representation in the beginning of the drift space after the lens, for $z=25.5$ cm, with $\varphi_0=2$ kV when the initial proton beam is non-parallel. The area in which the yield of transmitted protons is below 5% is designated by white color, the areas in which the yields are between 5 and 10%, 10 and 20%, 20 and 50%, 50 and 70% are designated by the increasing tones of gray color, respectively, and the area in which the yield is above 70% is designated by black color.

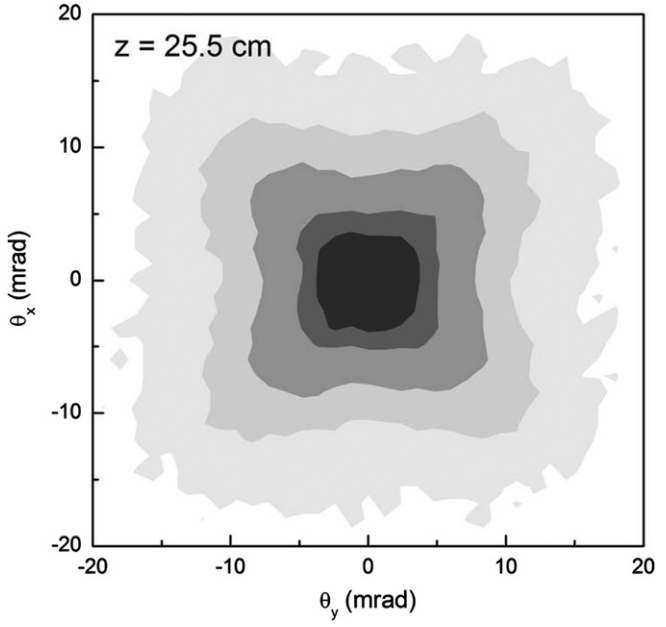

Fig. 13. Angular distribution of transmitted protons in the two-dimensional representation in the beginning of the drift space after the lens, for $z=25.5$ cm, with $\varphi_0=2$ kV when the initial proton beam is non-parallel. The area in which the yield of transmitted protons is below 5% is designated by white color, the areas in which the yields are between 5 and 10%, 10 and 20%, 20 and 50%, 50 and 70% are designated by the increasing tones of gray color, respectively, and the area in which the yield is above 70% is designated by black color.

protons in the beam core to the total number of focused protons in a transverse position plane and the ratio of the number of defocused protons in the beam core and the total number of defocused protons in a transverse position plane, respectively. It is evident that k_{cf} and k_{cd} decrease in the whole considered region of z, and that the decrease of k_{cd} is much more pronounced. It should be also mentioned that for $z=21.5$ cm the beam core contains 95.4% of the focused protons and 42.1% of the defocused protons, and that for $z=121.5$ cm these percentages are 84.8 and 9.8%, respectively.

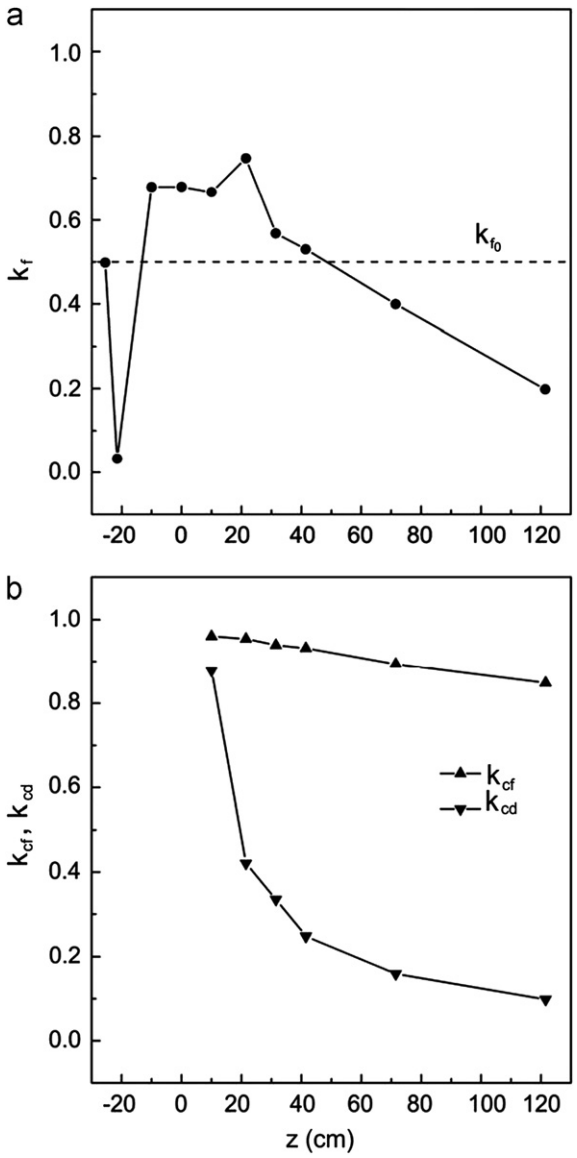

Fig. 14. Dependences of (a) the focusing coefficient of the lens, k_f, and (b) the confining coefficients of the lens for the focused and defocused protons, k_{cf} and k_{cd}, respectively, on z with $\varphi_0=2$ kV when the initial beam is non-parallel. k_{f0} is the initial focusing coefficient of the lens.

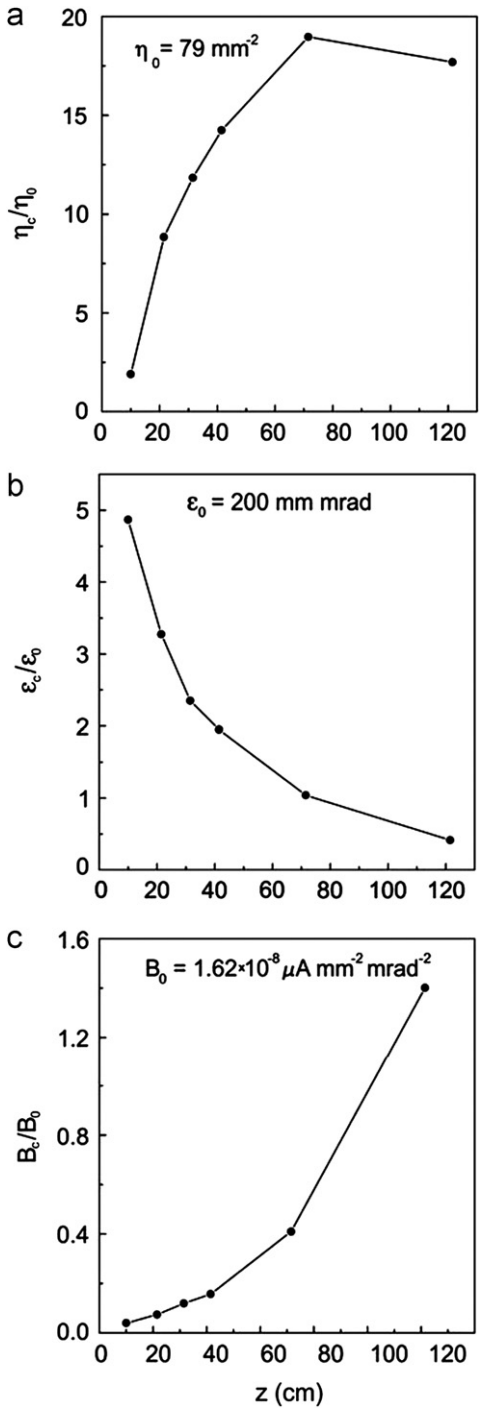

Fig. 15. Dependences of (a) the ratio of the density of the proton beam core and initial beam density, η_c/η_0, (b) the ratio of the vertical or horizontal emittance of the beam core and initial vertical or horizontal beam emittance, $\varepsilon_c/\varepsilon_0$, and (c) the ratio of the brightness of the beam core and initial beam brightness, B_c/B_0, on z with $\varphi_0=2$ kV when the initial proton beam is non-parallel.

Fig. 15 gives the ratio of the density of the proton beam core and initial beam density, η_c/η_0, the ratio of the vertical or horizontal emittance of the proton beam core and initial vertical or horizontal beam emittance [10], $\varepsilon_c/\varepsilon_0$, and the ratio of the brightness of the proton beam core and initial beam brightness [10], B_c/B_0, as a function of z between 10 and 121.5 cm; $\eta_0=79\ \mathrm{mm}^{-2}$, $\varepsilon_0=200$ mm mrad, and $B_0=1.62\times10^{-8}\ \mu\mathrm{A\,mm}^{-2}\,\mathrm{mrad}^{-2}$. In calculating the values of B_0 and B_c, we assumed that the incoming protons formed a beam bunch of the length of 10 μs. The resulting initial beam current was 6.4 nA.

It is clear that η_c has a maximum for $z=71.5$ cm. The maximal value of this beam parameter, being $1503\ \mathrm{mm}^{-2}$, is 19.0 times larger than η_0. Further, ε_c decreases in the whole considered region of z. At the lens exit, for $z=21.5$ cm, this beam parameter, being 655 mm mrad, is 3.3 times larger than ε_0, and at the chosen end of the drift space after the lens, being 83 mm mrad, it is 2.4 times smaller than ε_0. Finally, B_c increases in the whole considered region of z. At the lens exit, this beam parameter, being $1.20\times10^{-9}\ \mu\mathrm{A\,mm}^{-2}\,\mathrm{mrad}^{-2}$, is 13.5 times smaller than B_0, and at the chosen end of the drift space after the lens, being $2.28\times10^{-8}\ \mu\mathrm{A\,mm}^{-2}\,\mathrm{mrad}^{-2}$, it is 1.4 times larger than B_0.

4.4. Possible applications

The above presented results support the conclusions from our previous study [1] regarding the possible applications of square electrostatic rainbow lenses. These conclusions were based on "the confining ability of the rainbows" in the transverse position

plane and transmission angle plane. Such lenses as well as their multiplets can be applied for the effective definition and transportation of ion beams within accelerator facilities, including their preparation for collisions with each other, and for the creation of well-defined beams for research and development in condensed matter physics, biophysics, archeology and geology [1]. When compared to the corresponding quadrupole electrostatic lens [11], having a pair of opposite electrodes charged positively and the other pair negatively, a square electrostatic rainbow lens produces focused beams at larger distances [1]. Such a beam does not tend to reduce to a point.

Another possible application of square rainbow lenses can be for the efficient acceleration of ion beams—when they are biased by time-varying potentials. Our preliminary results show that the lens that has been considered here with the potential of its electrodes having the amplitude of 20 kV and frequency of 3 MHz provides the acceleration of the 10 keV proton beam up to about 50 keV [12]. The kinetic energy and its uncertainty of the accelerated beam are determined with a beam chopper placed in front of it and synchronized with it.

5. Conclusions

We have studied the transmission of parallel and non-parallel proton beams of the initial kinetic energy of 10 keV through a square electrostatic rainbow lens. The potential of the electrodes of the lens has been 2 kV. When the initial proton beam is parallel, the shapes of the spatial and angular distributions of transmitted protons inside the lens and in its exit region are determined fully by the shapes of the corresponding rainbow lines. At the lens exit the rainbow line in the transverse position plane bounds 99.5% of the focused protons and 62.9% of the defocused protons. In the beginning of the drift space after the lens the rainbow line in the transmission angle plane bounds 41.0% of the focused protons and 8.2% of the defocused protons.

When the initial proton beam is non-parallel, the spatial distributions of transmitted protons inside the lens and in the drift space after it are similar to the corresponding distributions when the beam is parallel. The chosen non-paralelism of the initial beam induces a moderate smearing of these distributions. At the lens exit the rainbow line in the transverse position plane bounds 92.0% of the focused protons and 45.7% of the defocused protons. The beam is separated into two components. One beam component, appearing as a beam core, is generated dominantly by the focused protons. Its boundary line in the transverse position plane can be very well approximated by a hypotrochoid. The other beam component is generated dominantly by the defocused protons. The angular distribution of transmitted protons in the beginning of the drift space after the lens also has the hypotrochoidal form.

After the lens exit, the focusing coefficient of the lens decreases, the confining coefficient of the lens for the focused protons decreases slightly, and the confining coefficient of the lens for the defocused protons decreases. At the lens exit the beam core contains 95.4% of the focused protons and 42.1% of the defocused protons, and at the chosen end of the drift space after the lens these percentages are 84.8 and 9.8%, respectively. In addition, after the lens exit, the density of the proton beam core has a maximum, the vertical or horizontal emittance of the beam core decreases, and the brightness of the beam core increases.

Acknowledgment

We acknowledge the support to this work provided by the Ministry of Education and Science of Serbia through project *Physics and Chemistry with Ion Beams*, No. III 45006.

References

[1] N. Nešković, I. Telečki, B. Bojović, S. Petrović, Nuclear Instruments and Methods in Physics Research A 635 (2011) 1.
[2] GetDP: A General Environment for the Treatment of Discrete Problems. ⟨http://www.geuz.org/getdp⟩.
[3] TetGen: A Quality Tetrahedral Mesh Generator and Three-Dimensional Delaunay Triangulator. ⟨http://tetgen.berlios.de⟩.
[4] N. Nešković, Physical Review B 33 (1986) 6030.
[5] N. Nešković, B. Perović, Physical Review Letters 59 (1987) 308.
[6] S. Petrović, L. Miletić, N. Nešković, Physical Review B 61 (2000) 184.
[7] N. Nešković, D. Borka, S. Šopić, S. Petrović, International Journal of Nonlinear Sciences and Numerical Simulation 11 (2010) 1131.
[8] D. Borka, S. Petrović, N. Nešković, Channeling of Protons through Carbon Nanotubes, Nova Science, New York, 2011.
[9] S.M. Lund, T. Kikuchi, R.C. Davidson, Physical Review Special Topics: Accelerators and Beams 12 (2009) 114801.
[10] S. Humphries Jr., Charged Particle Beams, John Wiley, New York, 1990.
[11] J.J. Livingood, Quadrupole lenses, in: Principles of Cyclic Particle Accelerators Van Nostrand, Princeton, New Jersey, 1961, pp. 299.
[12] N. Nešković, J.L. Ristić-Djurović, S. Petrović, P. Beličev, B. Rađenović, S. Ćirković, A.Ž. Ilić, A. Dobrosavljević, in preparation.